Fourier analysis of Bloch wave propagation in photonic crystals

Benoît Lombardet, L. Andrea Dunbar, Rolando Ferrini, and Romuald Houdré

Institut de Photonique et d'Electronique Quantique, Faculté des Sciences de Base, École Polytechnique Fédérale de Lausanne, CH-1015 Lausanne, Switzerland

Received September 23, 2004; revised manuscript received December 10, 2004; accepted December 29, 2004

The standard representation of an optical field propagating in a photonic crystal (PhC) is an electromagnetic Bloch wave. We present a description of these waves based on their Fourier transform into a series of electromagnetic plane waves. The contribution of each plane wave to the global energy and group velocity is detailed, and the valid domain of this decomposition is discussed. This description brings new insight to the fundamental properties of light propagation in PhCs. Most notably, it permits a continuous description of light propagation from the homogenous medium to the strongly modulated PhC case. It also provides an original physical understanding of negative refraction in PhCs and resolves inconsistencies that result from band folding.

OCIS codes: 130.2790, 260.2110.

1. INTRODUCTION

The propagation of an electromagnetic field in a periodic dielectric structure can be strongly modified when the lattice dimension is of the order of the light wavelength. Such periodic structures are called photonic crystals[1] (PhCs) and allow the control of light at the wavelength scale.[2] In particular, PhCs can forbid light propagation at certain energies, thus creating the so-called photonic bandgap[1,2] (PBG). Confining light in this way has created new means to tailor light–matter interaction[3,4] and has made PhCs promising materials for integrated optics.[5,6]

In the late 1970's, remarkable light dispersion properties of periodic media were demonstrated and studied.[7–9] Recently these interesting effects have been studied in PhCs,[10–12] paving the way for new concepts and applications. For example, phenomena such as negative refraction,[13–17] superprism,[18–20] and self-collimation[21–23] have been predicted and observed experimentally. In particular, several authors[11,14] have suggested that the group velocity and the wave vector of waves propagating in PhCs can be antiparallel for a certain frequency range. In this respect, PhCs can behave as left-handed materials[24] (LHMs), and a negative refractive index can be defined. However, Notomi *et al.*[11] have noticed that some definitions of refractive index lead to inconsistencies. For example, a homogenous medium regarded as a PhC with vanishing modulation retains an unphysical negative index value. Therefore, although negative refraction has been simulated and observed experimentally in PhCs, its physical understanding and connection with LHM properties still requires further investigation.

Owing to the periodic nature of PhC structures, electromagnetic Bloch waves are generally used to represent the propagation of the optical field in PhCs.[7] In this paper we present a description of these waves based on their Fourier transform into a series of electromagnetic plane waves. This description aims to give an intuitive understanding of these interesting effects and to answer some of the outstanding questions. In Section 2 we begin by describing the properties of Bloch waves in one-dimensional PhCs (1D-PhCs). After decomposing Bloch waves into series of plane waves, we then explain the contribution of each plane wave to the global energy and group velocity and discuss the valid domain of this decomposition. We also show how this approach resolves the inconsistencies observed for vanishing modulations. In Section 3 we generalize the results obtained in Section 2 to the two-dimensional (2D) case. Finally, in Section 4 we show that this description provides a physical understanding of the negative refraction that can occur at the interface between PhCs and homogenous media.

2. BLOCH WAVES IN ONE-DIMENSIONAL PHOTONIC CRYSTALS

Here we consider the propagation of an electromagnetic Bloch wave in a 1D-PhC. The alternating dielectric slabs have susceptibilities ε_1 and ε_2 and widths a_1 and a_2, respectively. The lattice period is thus $a=a_1+a_2$. We consider a wave propagating along the x direction perpendicular to the surface of the dielectric layers and linearly polarized in the y direction (Fig. 1). According to the Bloch theorem,[25] the corresponding magnetic field $\mathbf{H}_k$ satisfies the following relation:

$$\mathbf{H}_k(x) = H_k(x)\mathbf{e_z} = H_0 u_k(x)\exp(ikx)\mathbf{e_z}, \tag{1}$$

where H_0 is the field amplitude, $k \in [-\pi/a, \pi/a[$ is the wave number, and u_k is a normalized periodic function with period a. By use of the periodicity of u_k, H_k can be expanded in a series, i.e.,

$$H_k(x) = \sum_n h_{n(k)} H_0 \exp\left[i\left(k + n\frac{2\pi}{a}\right)x\right], \tag{2}$$

where each $h_{n(k)}$ is a dimensionless Fourier coefficient of the function u_k. Note that the normalization of u_k re-

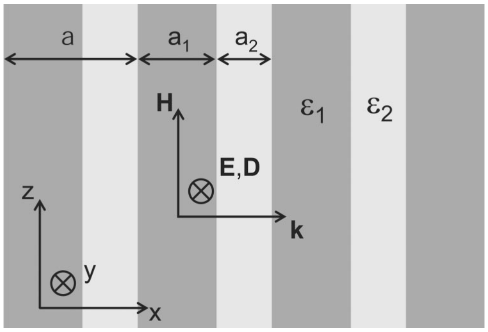

Fig. 1. Representation of the 1D PhC structure analyzed in this paper. The alternating dielectric slabs have susceptibilities ε_1 and ε_2 and widths a_1 and a_2. The lattice period is $a=a_1+a_2$. We consider electromagnetic Bloch waves propagating along the x direction perpendicular to the surface of the dielectric layers and linearly polarized in the y direction.

quires $\Sigma_n |h_{n(k)}|^2=1$. In Eq. (2) the spatial Fourier transform of the magnetic field is characterized by amplitude peaks $h_{n(k)}H_0$ located at the wave vectors $k_n=k+nK$, where $K=2\pi/a$. With the same arguments, the electric field $\mathbf{E}_k(x)=E_k(x)\mathbf{e_y}$ and the electric flux density $\mathbf{D}_k(x)=D_k(x)\mathbf{e_y}$ can also be expanded as a Fourier series:

$$E_k(x)=\sum_n E_{n(k)}\exp(ik_n x), \tag{3}$$

$$D_k(x)=\sum_n D_{n(k)}\exp(ik_n x). \tag{4}$$

To manipulate dimensionless quantities and thus simplify the following calculations, one can express the Fourier coefficients $E_{n(k)}$ and $D_{n(k)}$ without loss of generality as

$$E_{n(k)}=e_{n(k)}\mu_0 c H_0, \tag{5}$$

$$D_{n(k)}=d_{n(k)}H_0/c, \tag{6}$$

where c is the speed of light in a vacuum, μ_0 is the vacuum permeability, and $e_{n(k)}$ and $d_{n(k)}$ are dimensionless coefficients. Maxwell's equations $\nabla\times\mathbf{H}=-i\omega\mathbf{D}$ and $\nabla\times\mathbf{E}=i\omega\mu_0\mathbf{H}$, together with the constitutive relation $\mathbf{D}=\varepsilon_0\varepsilon\mathbf{E}$ and the Fourier expansion $1/\varepsilon_{(x)}=\Sigma_n\kappa_n\exp(inKx)$, yield the following relations between the coefficients $h_{n(k)}$, $e_{n(k)}$, and $d_{n(k)}$:

$$d_{n(k)}=h_{n(k)}\frac{k_n c}{\omega}, \tag{7}$$

$$h_{n(k)}=e_{n(k)}\frac{k_n c}{\omega}, \tag{8}$$

$$e_{n(k)}=\sum_{n'}\kappa_{n-n'}d_{n'(k)}. \tag{9}$$

Substituting Eqs. (7) and (9) into Eq. (8), we obtain the following relation for each integer n:

$$\sum_{n'}\kappa_{n-n'}k_n k_{n'}h_{n'(k)}=\left(\frac{\omega}{c}\right)^2 h_{n(k)}. \tag{10}$$

For $|n|\leqslant N$, Eq. (10) is the standard eigenvalue problem used in the plane-wave expansion (PWE) method for photonic band calculations.[26] For a given $k\in[-K/2,K/2[$, the $(2N+1)\times(2N+1)$ Hermitian matrix $\mathcal{M}_k^N(p,q)=\kappa_{p-q}(k+pK)(k+qK)$ has $2N+1$ positive eigenvalues $[(\omega_i/c)^2]_{i=1\ldots 2N+1}$. The corresponding eigenvectors $\mathcal{H}_{k,i}$ satisfy $\mathcal{M}_k^N\cdot\mathcal{H}_{k,i}=(\omega_i/c)^2\mathcal{H}_{k,i}$ and give the Fourier coefficients $h_{n(k,i)}$. In that the computation of photonic band diagrams requires only the eigenvalues, the corresponding eigenvectors are normally discarded. We will show that these components contain information that is essential for a comprehensive understanding of Bloch wave propagation. To do this, we start by describing the field properties in terms of the Fourier coefficients $h_{n(k)}$.

By use of Eqs. (7) and (8), the time–space average energy density $\langle\mathcal{E}_k\rangle_{t,s}$ of the Bloch wave can be developed as function of the $h_{n(k)}$ coefficients:

$$\langle\mathcal{E}_k\rangle_{t,s}=\left\langle\frac{1}{2}\frac{\mathbf{B}\cdot\mathbf{H}^*}{2}+\frac{1}{2}\frac{\mathbf{E}\cdot\mathbf{D}^*}{2}\right\rangle_s=\sum_n\frac{1}{2}\mu_0|h_{n(k)}|^2H_0^2. \tag{11}$$

Even though this expression could be simplified to $\frac{1}{2}\mu_0H_0^2$, the above form highlights the importance of the $h_{n(k)}$ coefficients. As it shows that $\langle\mathcal{E}_k\rangle_{t,s}$ can be decomposed into fractional energy densities $\mathcal{E}_{n(k)}=\frac{1}{2}\mu_0|h_{n(k)}|^2H_0^2$ corresponding to the energy density of an electromagnetic plane wave with the magnetic field amplitude $h_{n(k)}H_0$. Similarly, we develop the time–space average Poynting vector $\langle\mathbf{S_k}\rangle_{t,s}$:

$$\langle\mathbf{S}_k\rangle_{t,s}=\left\langle\mathrm{Re}\left(\frac{\mathbf{E}\times\mathbf{H}^*}{2}\right)\right\rangle_s=\sum_n\frac{1}{2}\mu_0c|h_{n(k)}|^2H_0^2\frac{\omega}{k_nc}\mathbf{e_x}.$$

The partial Poynting vector $\langle\mathbf{S}_{n(k)}\rangle=\frac{1}{2}\mu_0c|h_{n(k)}|^2H_0^2(\omega/k_nc)\mathbf{e_x}$ corresponds to the Poynting vector of an electromagnetic plane wave with the wave vector k_n and the magnetic field amplitude $h_{n(k)}H_0$.

The results obtained above are summarized in Table 1, and the corresponding relations for an electromagnetic plane wave are given for comparison. Using Maxwell's equations, we have obtained $\mathbf{E}_k$, $\mathbf{D}_k$, $\langle\mathcal{E}_k\rangle_{t,s}$, and $\langle\mathbf{S}_k\rangle_{t,s}$ in terms of the Fourier coefficients of $\mathbf{H}_k$. For each of these, when the nth component is considered individually, it always corresponds to the case of an electromagnetic plane wave with the wave vector k_n and the magnetic field amplitude $h_{n(k)}H_0$. This shows that a one-dimensional (1D) electromagnetic Bloch wave can be decomposed into a series of electromagnetic plane waves. Although this may seem obvious in the 1D case, in Section 2 we show that its generalization to the 2D case is not straightforward. The nth plane wave is characterized by the magnetic field amplitude $h_{n(k)}H_0$ and the wave vector k_n. Its contribution to the global field is given by $|h_{n(k)}|^2$, which is the ratio between the energy carried by this plane wave and the total energy carried by the Bloch wave. In spite of these similarities, the nth plane wave is not an electromagnetic plane wave, as it does not individually satisfy Maxwell's equations unlike the global Bloch wave,[7] i.e., is not an eigenvector of Eq. (10) for the eigenvalue ω. Therefore the

Table 1. Comparison between the Characteristics of the 1D Electromagnetic Bloch Wave and the 1D Electromagnetic Plane Wave

Wave Properties (1D)	Electromagnetic Bloch Wave	nth Component	Electromagnetic Plane Wave
Magnetic field	$\mathbf{H}_k=\Sigma_n \mathbf{H}_{n(k)}$	$\mathbf{H}_{n(k)}(x)=h_{n(k)}H_0 \exp(i\mathbf{k}_n x)\mathbf{e_z}$	$\mathbf{H}_k(x)=\exp(ikx)\mathbf{e_z}$
Electric field	$\mathbf{E}_k=\Sigma_n \mathbf{E}_{n(k)}$	$\mathbf{E}_{n(k)}(x)=\mu_0 c h_{n(k)}H_0 \frac{\omega}{k_n c}\exp(ik_n x)\mathbf{e_y}$	$\mathbf{E}_k(x)=\mu_0 c H_0 \frac{\omega}{kc}\exp(ikx)\mathbf{e_y}$
Time–space-averaged energy density	$\langle \mathcal{E}_k\rangle_{t,s}=\Sigma_n \mathcal{E}_{n(k)}=\frac{1}{2}\mu_0 H_0^2$	$\mathcal{E}_{n(k)}=\frac{1}{2}\mu_0 \lvert h_{n(k)}\rvert^2 H_0^2$	$\langle \mathcal{E}_k\rangle_{t,s}=\frac{1}{2}\mu_0 H_0^2$
Time–space-averaged Poynting vector	$\langle \mathbf{S}_k\rangle_{t,s}=\Sigma_n \mathbf{S}_{n(k)}$	$\mathbf{S}_{n(k)}=\frac{1}{2}\mu_0 \lvert h_{n(k)}\rvert^2 H_0^2 \frac{\omega}{k_n}\mathbf{e_x}$	$\langle \mathbf{S}_k\rangle_{t,s}=\frac{1}{2}\mu_0 H_0^2 \frac{\omega}{k}\mathbf{e_x}$
Group velocity	$\mathbf{v_g}=\Sigma_n \lvert h_{n(k)}\rvert^2 \mathbf{v_n}$	$\mathbf{v_n}=\frac{\omega}{k_n}\mathbf{e_x}$	$\mathbf{v_g}=\frac{\omega}{k}\mathbf{e_x}$

nth plane wave is not an eigenvalue of the field equations and exists only as part of the Bloch wave.

Finally, we develop the group velocity $\mathbf{v_g}$, which is equal in periodic media[27] to the energy velocity $\mathbf{v_e}$:

$$\mathbf{v_g}=\mathbf{v_e}=\frac{\langle \mathbf{S}_k\rangle_{t,s}}{\langle \mathcal{E}_k\rangle_{t,s}}=\sum_n \lvert h_{n(k)}\rvert^2 \frac{\omega}{k_n}\mathbf{e_x}. \tag{12}$$

The group velocity is simply given by the sum of the group velocities $\mathbf{v}_n=\omega/k_n$ of the plane waves weighted by their energetic contribution $\lvert h_{n(k)}\rvert^2$. The Fourier decomposition of a Bloch wave is illustrated in Fig. 2. The nth plane wave is represented by a disk located at the point (k_n,u): The gray level of the disk indicates the energetic contribution of this plane wave (black$\rightarrow 1$, white$\rightarrow 0$). The contribution to the total group velocity $\mathbf{v_g}$ is indicated by an arrow whose length is proportional to $\lvert h_{n(k)}\rvert^2\omega/k_n$. The positive and negative parts of the jth Brillouin zone are labeled j^{+}BZ and j^{-}BZ, respectively. In this example, $k_0=k$, $k_{-1}=k-K$, and $k_1=k+K$ are in the first, second, and third BZs, respectively.

Having established the basic description of Bloch waves and their decomposed plane waves in a periodic material, we now look at their propagation in three different 1D-PhCs with varying index modulations: $\Delta n=0$, 1.2, and 2.3. The parameters of the 1D-PhCs are as follow: homogenous medium ($\varepsilon_1=\varepsilon_2=4.67$), weakly modulated 1D-PhC ($\varepsilon_1=2.43$ and $\varepsilon_2=7.62$), and strongly modulated 1D-PhC ($\varepsilon_1=1$ and $\varepsilon_2=11$). To ensure we examine only the difference arising from the magnitude of the modulation, all other parameters remain identical, i.e., $a_1=a_2=a/2$ and $\langle n\rangle=2.16$ (average refractive index). Using the PWE method, we plot in Fig. 3 (seen on next page) the dispersion diagrams for the first three bands of the 1D-PhCs. The two modulated 1D-PhCs exhibit two PBGs splitting the energy range into three allowed photonic bands (I, II, and III). A Bloch wave with the wave vector k located in band X=I, II, or III is labeled X_k.

The Bloch waves propagating in the positive x direction of the three different 1D-PhCs are represented in Fig. 4 (the representation is the same as in Fig. 2). The arrows indicating the contributions to the global group velocity are drawn for waves $\mathrm{I}_{0.25}$, $\mathrm{I}_{0.5}$, $\mathrm{II}_{-0.5}$, and $\mathrm{II}_{-0.25}$.

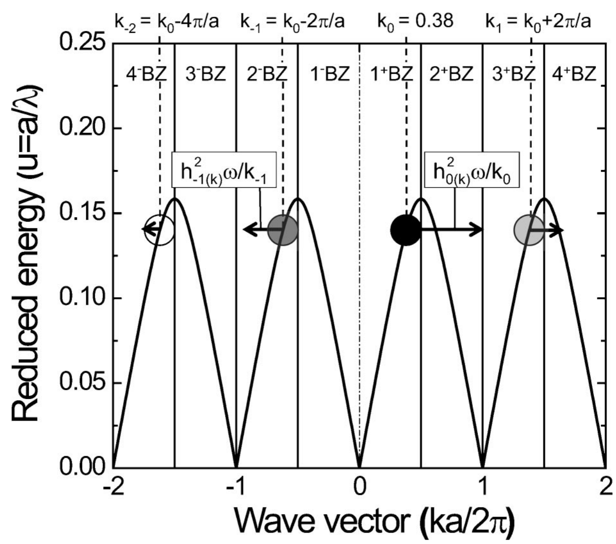

Fig. 2. Graphical representation of a Bloch wave with energy $u=0.14$ and wave vector $k=0.38$ propagating in a 1D-PhC. The band diagram (black curve) of the 1D-PhC is repeated in the different Brillouin zones. The plane waves that collectively form this Bloch wave are represented by disks located at the points (k_n,u). The gray level of each disk indicates the energetic contribution of the corresponding plane wave, i.e., the ratio between the energy carried by this plane wave and the total energy carried by the Bloch wave (black$\rightarrow 1$, white$\rightarrow 0$). The contribution of the nth plane wave to the total group velocity $\mathbf{v_g}$ of the Bloch wave is indicated by an arrow whose length is proportional to $\lvert h_{n(k)}\rvert^2\omega/k_n$. The vectorial sum of all these arrows gives $\mathbf{v_g}$.

In the homogenous medium [Fig. 4(a)], the solution to Maxwell's equations at energy ω is an electromagnetic plane wave with wave vector $k=\sqrt{\varepsilon}\omega/c$. This plane wave can be regarded as a particular Bloch wave for which $h_{n(k)}$ is equal to 1 for a unique integer n^* and 0 otherwise. The corresponding representation is characterized by a single black disk ($h_{n^*(k)}=1$) located at the point (k_{n^*},u), where $k_{n^*}=\sqrt{\varepsilon}\omega/c$. When all the waves are represented on the global diagram, their black disks overlap to draw the standard dispersion line of an homogeneous medium. Hence this representation of Bloch waves gives self-consistent results when the PWE method is applied to an homogeneous medium, represented here as a 1D-PhC with zero index contrast. The Bloch wave decomposition here is totally dominated by the single plane-wave solution of Maxwell's equations. The index of this component is labeled n^*: $n^*=1$ for Bloch waves within the first band, $n^*=2$ for Bloch waves within the second band, $n^*=3$ for Bloch waves within the third band, and so forth.

When a weak modulation is introduced into the PhC, as is the case in the weakly modulated 1D-PhC [Fig. 4(b)], only the vicinity of the BZ boundaries is affected. Inside the transmission bands, the Bloch wave remains similar to the plane-wave n^* solution of the homogeneous medium. For example, more than 98% of the total energy of Bloch wave $\mathrm{I}_{0.25}$ is carried by plane wave $n^*=1$. When the band edge is approached, some of the Bloch wave energy is transmitted from plane wave n^* to plane wave n^*-1. At the band edge, the energy is equally distributed between these two contrapropagating plane waves. The resulting Bloch waves are the symmetric and antisymmetric standing waves $\mathrm{I}_{0.5}$ and $\mathrm{II}_{-0.5}$. Because $k_{n^*}=-k_{n^*-1}(=K/2)$, their group velocities are zero; see Eq. (12).

For the strongly modulated 1D-PhC [Fig. 4(c)], the large increase of the index contrast affects the whole transmission band. The energy is now distributed between several plane waves even in the middle of the bands, and the PBGs are larger. Yet plane wave n^* still dominates the decomposition inside the bands. For example, plane wave n^* carries 70% of the total energy of Bloch wave $\mathrm{II}_{-0.25}$, whereas plane waves n^*-1 and n^*-2 correspond just to 12% and 2%. Finally, it should be noted that the plane wave n^* is not necessarily located in the first BZ. In fact, this wave lies within the second BZ for Bloch waves of the second transmission band, within the third BZ for Bloch waves of the third transmission band, etc. This intrinsic property is essential for a consistent description of Bloch waves in PhCs.

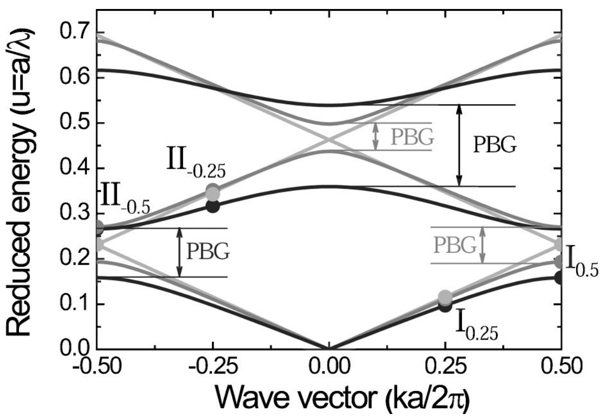

Fig. 3. Photonic band diagrams for three different 1D-PhCs with increasing index contrasts. The light gray, dark gray, and black curves denote the homogenous medium ($\varepsilon_1=\varepsilon_2=4.67$), the weakly modulated 1D-PhC ($\varepsilon_1=2.43$ and $\varepsilon_2=7.62$), and the strongly modulated 1D-PhC ($\varepsilon_1=1$ and $\varepsilon_2=11$), respectively. The PBGs of the weakly and strongly modulated 1D-PhCs are indicated, as are four characteristic Bloch waves: $\mathrm{I}_{0.25}$, $\mathrm{II}_{-0.25}$, $\mathrm{I}_{0.5}$, and $\mathrm{II}_{-0.5}$. These waves located in the middle and at the edges of the first and the second bands are often used as examples in the text.

The previous description brings new insight for the understanding of light propagation in PhCs. In particular, it clearly describes the direction of the group velocity and the transition from the homogeneous medium to the strongly modulated 1D-PhC. There is one last aspect we wish to consider before generalizing our results to the 2D case, that is, the definition of a phase refractive index for a Bloch wave. Dowling and Bowden[28] first defined it by using the textbook formula $n_p=|k|c/\omega$, where k is taken from the first BZ. They obtained the anomalous behavior sketched in Fig. 5(a), which predicts small refractive indices for PhCs. Notomi[11] noticed that this method leads to abnormal results for a homogeneous medium and concluded that this definition has no physical meaning. Using the description developed in this paper, we can remove this inconsistency. Having shown that a Bloch wave is composed of plane waves propagating at their own phase velocities $\mathbf{v}_n=\omega/k_n$, we conclude that no global phase-front velocities can be physically attributed to the global Bloch wave. The main flaw in Dowling and Bowden's definition lies in attributing the phase velocity $\mathbf{v}_0=\omega/k_0$ of the plane wave located in the first BZ. To illustrate this, we consider the phase velocity of plane wave $\mathrm{II}_{-0.25}$ in the homogeneous medium. Dowling and Bowden's definition assigns it the wave vector $k=k_0=-0.25$, although this standard plane wave is entirely described by the wave vector $k_{n^*}=k_1=0.75$. Thus the small values of the phase refractive index observed in Fig. 5(a) results from the artificial band folding and are not physical.

We conclude that no phase index can be physically assigned to Bloch waves as these waves possess many phase

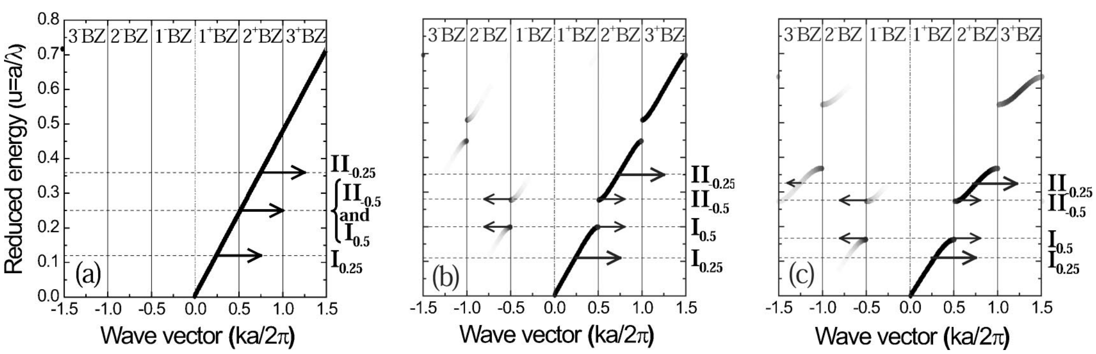

Fig. 4. Graphical representation of the Bloch waves that propagate in the positive x direction of (a) the homogenous medium, (b) the weakly modulated 1D-PhC, and (c) the strongly modulated 1D-PhC. The Bloch waves have the same representation as in Fig. 2: The circles of adjacent Bloch waves overlap, and the arrows indicating the contributions to the group velocity are drawn for Bloch waves $\mathrm{I}_{0.25}$, $\mathrm{I}_{0.5}$, $\mathrm{II}_{-0.5}$, and $\mathrm{II}_{-0.25}$. We note that the dominant plane wave is located in the first BZ for the first band, in the second BZ for the second band, and forth on.

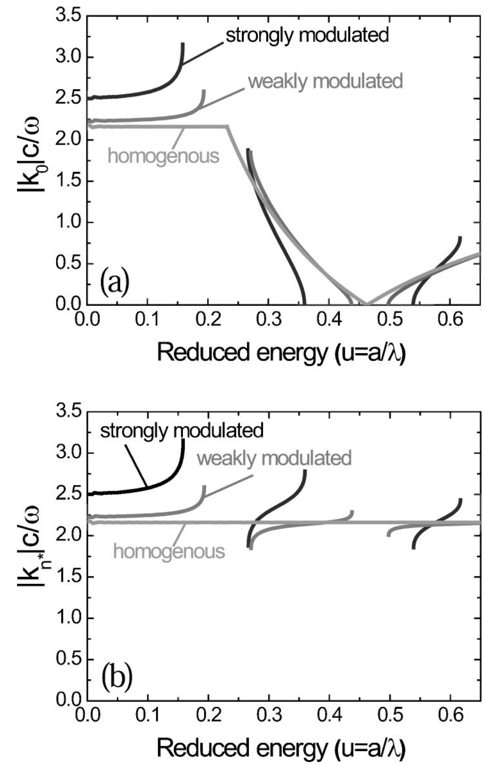

Fig. 5. Phase index $|k|c/\omega$ versus energy for the investigated 1D-PhCs. The light gray, dark gray, and black curves denote, respectively, the homogenous medium, the weakly modulated 1D-PhC, and the strongly modulated 1D-PhC. (a) The wave vector k used in the calculation corresponds to the wave vector $k=k_0$ of the plane wave located in the first BZ. From this definition, meaningless values are observed for the phase index in PhCs[27] and the standard results for an homogenous medium[11] are not recovered. (b) The wave vector k corresponds to the wave vector k_{n^*} of the plane wave that dominates the Fourier decomposition of the Bloch wave.

velocities. Finally, it should be noted that one can obtain self-consistent results for the transition from a homogeneous medium to a PhC by considering the quantity $|k_{n^*}|c/\omega$ instead of $|k_0|c/\omega$ [Fig. 5(b)]. However, this quantity characterizes only the velocity of the dominant phase front of the Bloch wave and is not a useful value.

3. PROPAGATION OF BLOCH WAVES IN TWO-DIMENSIONAL PHOTONIC CRYSTALS

In this section the preceding results are generalized to the 2D case. The structure consists of a square lattice of dielectric rods with susceptibility ε_2 embedded in a dielectric medium with susceptibility ε_1 (Fig. 6). The period is a, and the rod radius is r. The filling factor is $f=\pi r^2/a^2$, and the average susceptibility $\langle\varepsilon\rangle$ is given by $\langle\varepsilon\rangle=f\varepsilon_1+(1-f)\varepsilon_2$. The z axis is parallel to the rods, and only Bloch waves propagating in the xy plane are considered. A typical dispersion diagram of such a structure is depicted in Fig. 7. In the following analysis, we will consider TM-polarized waves ($\mathbf{E}\|\mathbf{e_z}$).

As in the 1D case, the different fields satisfy the Bloch's theorem and can be expanded as a Fourier series:

$$\mathbf{H_k}(\mathbf{r})=\sum_{n,m}\mathbf{h}_{n,m(\mathbf{k})}H_0\exp[i(\mathbf{k}+\mathbf{G}_{n,m})\cdot\mathbf{r}], \tag{13}$$

$$\mathbf{E_k}(\mathbf{r})=\sum_{n,m}\mathbf{e}_{n,m(\mathbf{k})}\mu_0 cH_0\exp[i(\mathbf{k}+\mathbf{G}_{n,m})\cdot\mathbf{r}], \tag{14}$$

$$\mathbf{D_k}(\mathbf{r})=\sum_{n,m}\mathbf{d}_{n,m(\mathbf{k})}\frac{H_0}{c}\exp[i(\mathbf{k}+\mathbf{G}_{n,m})\cdot\mathbf{r}], \tag{15}$$

where H_0, c, μ_0, $\mathbf{r}$, and $\mathbf{k}$ are defined as in the 1D case; $\mathbf{G}_{n,m}$ are the reciprocal vectors; and $\mathbf{h}_{n,m(\mathbf{k})}$, $\mathbf{e}_{n,m(\mathbf{k})}$, and $\mathbf{d}_{n,m(\mathbf{k})}$ are dimensionless vectors. Note that for TM polarization, $\mathbf{e}_{n,m(\mathbf{k})}=e_{n,m(\mathbf{k})}\mathbf{e_z}$ and $\mathbf{d}_{n,m(\mathbf{k})}=d_{n,m(\mathbf{k})}\mathbf{e_z}$. Maxwell's equation $\nabla\times\mathbf{H}=-i\omega\mathbf{D}$ and $\nabla\times\mathbf{E}=i\omega\mu_0\mathbf{H}$, together with the constitutive relation $\mathbf{D}=\varepsilon_0\varepsilon\mathbf{E}$ and the Fourier expansion $1/\varepsilon_{(\mathbf{r})}=\Sigma_{n,m}\kappa_{n,m}\exp(i\mathbf{G}_{n,m}\mathbf{r})$, lead to the following vectorial relations:

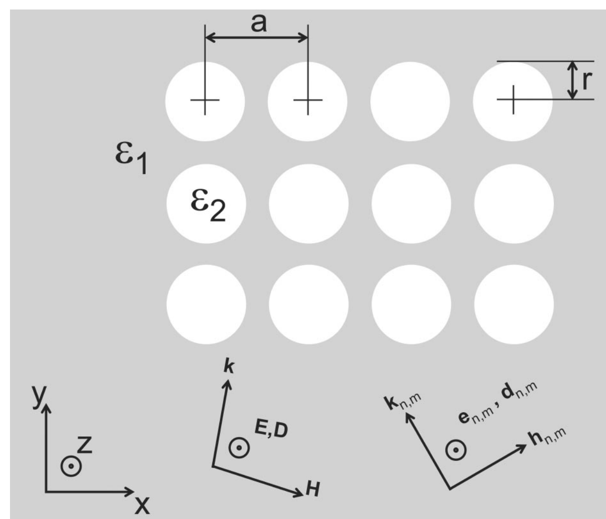

Fig. 6. Top view of the investigated 2D-PhC. A square lattice of dielectric rods with susceptibility ε_2 is embedded in a dielectric medium with susceptibility ε_1. The lattice period is a, and the rod radius is r. We consider TM-polarized ($\mathbf{E}\|\mathbf{e_z}$) Bloch waves propagating in the xy plane perpendicular to the rods.

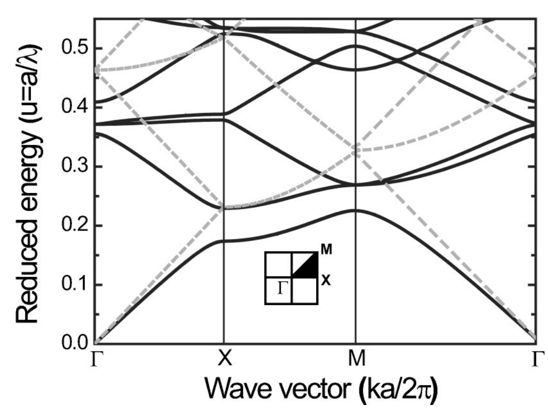

Fig. 7. Photonic band diagrams of an homogenous medium ($\varepsilon_1=\varepsilon_2=4.67$, dashed gray curve) and a strongly modulated 2D-PhC ($\varepsilon_1=1$ and $\varepsilon_2=11$, black curve). For comparison, both of them have the same filling factor $f=50\%$ and the same average refractive index $\langle n\rangle=2.16$. The three highly symmetric points Γ, M, and X of the square lattice are indicated.

Table 2. Comparison between the Characteristics of the 2D Electromagnetic Bloch Wave and the 2D Electromagnetic Plane Wave

Wave Properties (2D)	Electromagnetic Bloch Wave	(n,m)th Component	Electromagnetic Plane Wave
Magnetic field	$\mathbf{H_k}=\Sigma_{n,m}\mathbf{H}_{n,m(\mathbf{k})}$	$\mathbf{H}_{n,m(\mathbf{k})}(\mathbf{r})=\mathbf{h}_{n,m(\mathbf{k})}\mathbf{H}_0 \exp(i\mathbf{k}_{n,m}\cdot\mathbf{r})$	$\mathbf{H_k}(\mathbf{r})=\mathbf{H_0}\exp(i\mathbf{k}\cdot\mathbf{r})$
Electric field	$\mathbf{E_k}=\Sigma_{n,m}\mathbf{E}_{n,m(\mathbf{k})}$	$\mathbf{E}_{n,m(\mathbf{k})}(\mathbf{r})=\mu_0\lvert\mathbf{h}_{n,m(\mathbf{k})}\rvert H_0\frac{\omega}{\lvert\mathbf{k}_{n,m}\rvert}\exp(i\mathbf{k}_{n,m}\cdot\mathbf{r})\mathbf{e_z}$	$\mathbf{E_k}(\mathbf{r})=\mu_0 H_0\frac{\omega}{\lvert\mathbf{k}\rvert}\exp(i\mathbf{k}\cdot\mathbf{r})\mathbf{e_z}$
Time-space-averaged energy density	$\langle\mathcal{E}_\mathbf{k}\rangle_{t,s}=\Sigma_{n,m}\mathcal{E}_{n,m(\mathbf{k})}=\frac{1}{2}\mu_0 H_0^2$	$\mathcal{E}_{n,m(\mathbf{k})}=\frac{1}{2}\mu_0\lvert\mathbf{h}_{n,m(\mathbf{k})}\rvert^2 H_0^2$	$\langle\mathcal{E}_\mathbf{k}\rangle_{t,s}=\frac{1}{2}\mu_0 H_0^2$
Time-space-averaged Poynting vector	$\langle\mathbf{S_k}\rangle_{t,s}=\Sigma_{n,m}\mathbf{S}_{n,m(\mathbf{k})}$	$\mathbf{S}_{n,m(\mathbf{k})}=\frac{1}{2}\mu_0\lvert\mathbf{h}_{n,m(\mathbf{k})}\rvert^2 H_0^2\frac{\omega}{\mathbf{k}_{n,m}^2}\mathbf{k}_{n,m}$	$\langle\mathbf{S_k}\rangle_{t,s}=\frac{1}{2}\mu_0 H_0^2\frac{\omega}{\mathbf{k}^2}\mathbf{k}$
Group velocity	$\mathbf{v_g}=\Sigma_{n,m}\lvert\mathbf{h}_{n,m(\mathbf{k})}\rvert^2\mathbf{v}_{n,m}$	$\mathbf{v}_{n,m}=\frac{\omega}{\mathbf{k}_{n,m}^2}\mathbf{k}_{n,m}$	$\mathbf{v_g}=\frac{\omega}{\mathbf{k}^2}\mathbf{k}$

$$\mathbf{d}_{n,m(\mathbf{k})}=-\frac{\mathbf{k}_{n,m}c}{\omega}\times\mathbf{h}_{n,m(\mathbf{k})}, \tag{16}$$

$$\mathbf{h}_{n,m(\mathbf{k})}=\frac{\mathbf{k}_{n,m}c}{\omega}\times\mathbf{e}_{n,m(\mathbf{k})}, \tag{17}$$

$$\mathbf{e}_{n,m(\mathbf{k})}=\sum_{n',m'}\kappa_{n-n',m-m'}\mathbf{d}_{n',m'(\mathbf{k})}, \tag{18}$$

where $\mathbf{k}_{n,m}=\mathbf{k}+\mathbf{G}_{n,m}$. Substituting Eqs. (16) and (17) into Eq. (18) gives the equation for the coefficients $e_{n,m(\mathbf{k})}$:

$$\sum_{n',m'}\kappa_{n-n',m-m'}\lvert\mathbf{k}_{n,m}\rvert\lvert\mathbf{k}_{n',m'}\rvert\frac{e_{n',m'(\mathbf{k})}}{\lvert\mathbf{k}_{n,m}\rvert}=\left(\frac{\omega}{c}\right)^2\frac{e_{n,m(\mathbf{k})}}{\lvert\mathbf{k}_{n,m}\rvert}. \tag{19}$$

For $|n|$, $|m|\leqslant N$, Eq. (19) is the standard eigenvalue equation used in the PWE method to compute the dispersion relations of TM-polarized waves in 2D-PhCs.[26] The eigenvectors give the coefficients $e_{n,m(\mathbf{k})}/|\mathbf{k}_{n,m}|$ from which the vectors $\mathbf{e}_{n,m(\mathbf{k})}$ can be easily deduced. The vectors $\mathbf{h}_{n,m(\mathbf{k})}$ and $\mathbf{d}_{n,m(\mathbf{k})}$ can then be calculated[29] from Eqs. (17) and (16).

To generalize the 1D-PhC results, we must describe the field properties in terms of the vectors $\mathbf{h}_{n,m(\mathbf{k})}$. A simple calculation leads to the expressions reported in Table 2. As in the 1D case, these results show that a TM-polarized Bloch wave can be decomposed into a Fourier series of TM-polarized plane waves. Note, however, that the generalization of this result for TE-polarized waves is not straightforward.[30] The (n,m)th plane wave is characterized by the magnetic field amplitude $\mathbf{h}_{n,m(\mathbf{k})}H_0$ and the wave vector $\mathbf{k}_{n,m}$. Its contribution to the global field is given by the quantity $|\mathbf{h}_{n,m(\mathbf{k})}|^2$, which is the ratio between the energy carried by this plane wave and the total energy carried by the Bloch wave. As in the 1D case, this pseudoelectromagnetic plane wave does not necessarily satisfy Maxwell's equations. Therefore the (n,m)th plane wave is not an eigenvalue of the field equations and exists only in the PhC as part of the Bloch wave. We illustrate the decomposition with an example in Fig. 8. In Fig. 8(a) the (n,m)th plane wave is represented by a disk located at $\mathbf{k}_{n,m}$: The gray level of the disk indicates the energetic contribution $|\mathbf{h}_{n,m(\mathbf{k})}|^2$ of this plane wave (black $\rightarrow 1$, white $\rightarrow 0$). The group velocity is given by the vectorial sum of the phase velocities $\omega\mathbf{k}_{n,m}/\mathbf{k}_{n,m}^2$, weighted by the energetic contributions $|\mathbf{h}_{n,m(\mathbf{k})}|^2$ of the corresponding plane waves. Because each term can be physically interpreted, this approach provides an intuitive understanding of the direction of the group velocity as illustrated in Fig. 8(b). From the center of the disk, the vector $|\mathbf{h}_{n,m(\mathbf{k})}|^2\omega\mathbf{k}_{n,m}/\mathbf{k}_{n,m}^2$ shows the contribution of the (n,m)th plane wave to the global group velocity. The higher-order BZs are indicated with dashed lines. In this example, $\mathbf{k}_{0,0}$, $\mathbf{k}_{-1,0}$, $\mathbf{k}_{0,-1}$, and $\mathbf{k}_{0,1}$ are in the first, second, third, and fourth BZs, respectively.

To illustrate this description, we consider the propagation of Bloch waves in 2D-PhCs with different index contrasts: a homogenous medium, a weakly modulated 2D-PhC, and a strongly modulated 2D-PhC. Their respective susceptibilities are the same as in the 1D case, and they all have the same filling factor $f=50\%$ and average index $\langle n\rangle=2.16$. Generalizing Fig. 4, we study in Fig. 9 the effects of the modulation by looking at the energetic composition of the Bloch waves located in the first three bands of these 2D-PhCs. Each Bloch wave is represented as described in Fig. 8. Here the disks of adjacent Bloch waves overlap, and the contributions to the group velocity are not indicated.

In an homogeneous medium, which is represented by a 2D-PhC with zero index contrast [Fig. 9(a)], the plane-wave solution of Maxwell's equation is artificially distributed in bands according to the position of the wave vector $\mathbf{k}$. When $\mathbf{k}$ is located in the first, second, or third BZ, the wave is assigned to the first, second, or third band, respectively. As in the 1D case, each of these particular Bloch waves is represented by a single black dot located at $\mathbf{k}$. Therefore the global graphical representations of the first, second, and third bands are simply the first, second, and third BZs filled in black.

The introduction of a weak modulation [Fig. 9(b)] does not strongly influence the solutions except at the BZ boundaries, i.e., the Fourier decomposition is still largely dominated by the plane-wave (n^*,m^*) solution in the homogenous medium case. At the vicinity of the BZ boundaries, the decomposition is dominated by the two plane waves located in the neighboring BZs. For example, Bloch wave $I_{0.47,0}$ lies in the first band with its dominant plane wave $[\mathbf{k}_{n^*,m^*}=(0.47,0)]$ located in the first BZ; see Fig. 9(b). Because this Bloch wave lies in the vicinity of the second BZ border, part of its energy is carried by the plane wave located in the second BZ $[\mathbf{k}_{n^*-1,m^*}=(-0.53,0)]$. At the border the energy of the global Bloch wave is equally distributed between the two dominant plane waves.

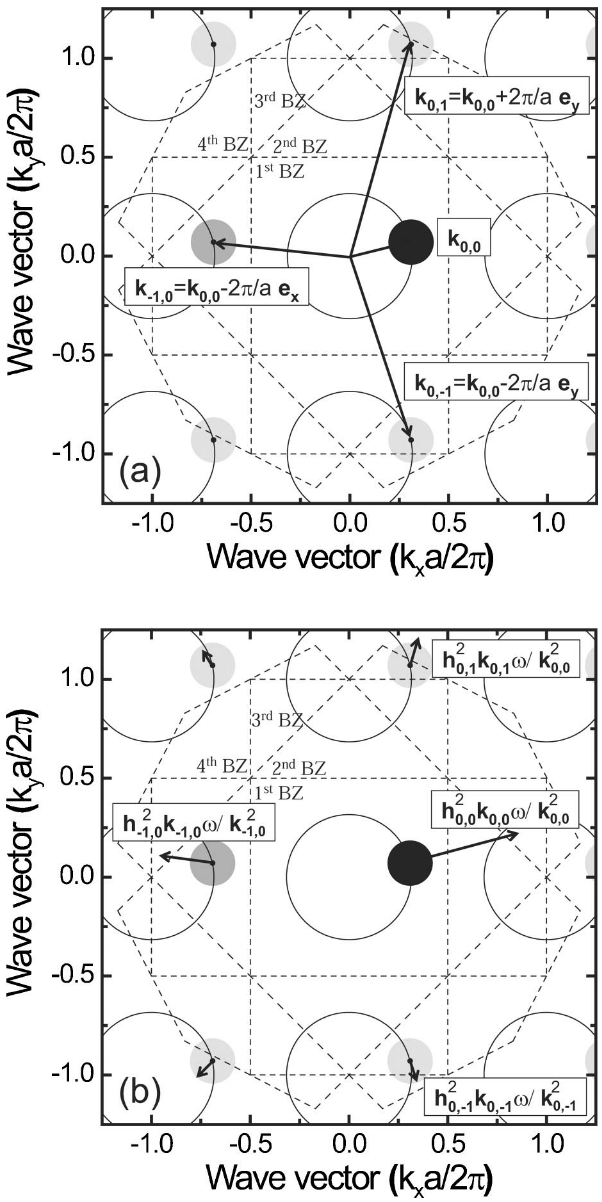

Fig. 8. Graphical representation of a Bloch wave propagating in a 2D-PhC. This wave with wave vector $\mathbf{k}=(0.3,0.1)$ and energy $u=0.123$ is located in the first band. The BZ boundaries are represented by dashed lines. The black circles indicate the equifrequency surfaces for the energy $u=0.123$. (a) The plane waves that collectively form the Bloch wave are represented by disks located at their respective wave vectors $\mathbf{k}_{n,m}$. The gray level of each disk indicates the energetic contribution of the corresponding plane wave, i.e., the ratio between the energy carried by this plane wave and the total energy carried by the Bloch wave (black$\rightarrow$1, white$\rightarrow$0). (b) The contribution of the (n,m)th plane wave to the total group velocity $\mathbf{v_g}$ of the Bloch wave is indicated by a black arrow whose length is proportional to $|\mathbf{h}_{n,m(\mathbf{k})}|^2\mathbf{k}_{n,m}\omega/\mathbf{k}^2_{n,m}$. The vectorial sum of all these arrows gives $\mathbf{v_g}$.

Finally, the strongly modulated 2D-PhC [Fig. 9(c)] confirms the importance of the dominant plane wave (n^*,m^*) in the 2D case. Inside the bands, this wave still dominates the Fourier decomposition and carries the largest part of the Bloch wave energy; this characteristic is essential to understand the physics of Bloch wave propagation in 2D-PhCs.

The analysis in terms of the equifrequency surfaces (EFSs) is a common way to investigate the propagation direction of Bloch waves in 2D-PhCs; their group velocities are given by the gradient vectors of these curves.[10] Normally, the EFSs are calculated for each band and drawn inside the first BZ, thus characterizing each wave with the wave vector $\mathbf{k}=\mathbf{k}_{0,0}$. As an example, the EFSs of the first and second bands of the homogenous medium are represented in Figs. 10(a) and 10(b), respectively. In the first band, this diagram shows the expected concentric circles of the homogeneous medium. However, nonintuitive curves pointing inward are obtained for the second band. This is a consequence of characterizing Bloch waves according to the wave vector of the first BZ (band folding).

As an illustration, we consider the plane wave with energy $u=0.3$ that propagates in the negative x direction in the homogeneous medium. In the folded diagram, this particular Bloch wave is identified by the wave vector $\mathbf{k}=\mathbf{k}_{0,0}=(0.352,0)$. However, as shown above, this vector has no physical meaning in that the unique (and therefore dominant) Fourier component of this wave is characterized by the wave vector $\mathbf{k}_{n^*,m^*}=(-0.648,0)$ and is located in the second BZ. When this more physical approach of characterizing Bloch waves through their dominant wave vector $\mathbf{k}_{n^*,m^*}$ is adopted, the EFS of the second band is represented in the second BZ. With this representation, we obtain the projection in the second BZ of the concentric circles of the homogeneous medium [Fig. 10(c)] pointing outward as in the first BZ.

Thus, by our drawing the EFSs of the various bands in their respective BZs, the global diagram exhibits the expected EFS of an homogenous medium [Fig. 11(a)]. The same method can be applied to construct the global EFS diagrams of the weakly and strongly modulated 2D-PhCs [Figs. 11(b) and 11(c)]. With this pictorial representation, the three cases can be compared easily. The modulation transforms continuously the disks of the homogeneous medium to the segmental disks of the modulated PhC with no abrupt modification of the EFS. In particular, all the EFSs point outward, contrary to the common belief that in the second band of PhCs they point inward.[11,18,31] This unusual property resulted from the enforced representation of the EFS in the first BZ and erroneously showed the EFS of the second band of the homogenous medium pointing inward; see Fig. 10(b). Therefore the negative curvature of the EFS is a result of the artificial band folding and has no physical meaning. Thus it should not be invoked to explain the left-handed behavior of PhCs.

Left-handed materials (LHMs) are generally characterized by the negative sign of the scalar product $\mathbf{k}\cdot\mathbf{v_g}$, where $\mathbf{k}$ is the wave vector and $\mathbf{v_g}$ is the group velocity. To calculate this scalar product, we must assign a single wave vector $\mathbf{k}$ to the wave. Unfortunately, Bloch waves

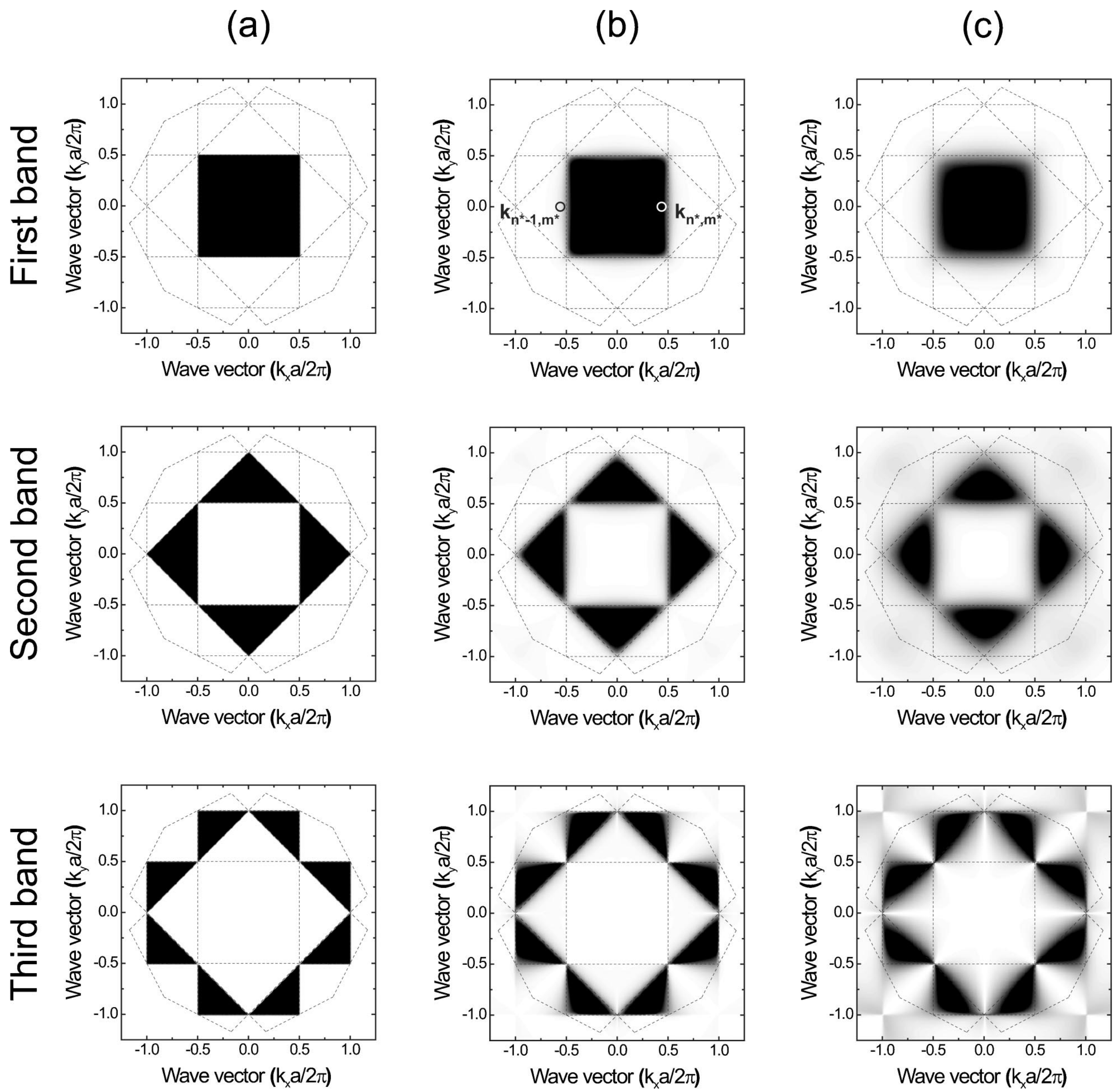

Fig. 9. Graphical representation of the TM-polarized Bloch waves that propagate in (a) the homogenous medium, (b) the weakly modulated 2D-PhC, and (c) the strongly modulated 2D-PhC. We consider only the waves located in the first (I), second (II), and third (III) band. The BZ boundaries are represented by dashed lines. Each Bloch wave is represented as described in Fig. 8: The circles of adjacent Bloch waves overlap, and the contributions to $\mathbf{v_g}$ are not indicated. We observe that the dominant plane wave is located in the first BZ for the first band, in the second BZ for the second band, and so forth. Note that the contributions of the other plane waves become larger as the modulation is increased.

are composed of many plane waves whose wave vectors are all necessary to describe the global Bloch wave. Although there is no *a priori* reason to favor one of them, the wave vector $\mathbf{k}=\mathbf{k}_{0,0}$ located in the first BZ is generally adopted to characterize Bloch waves in PhCs. Let us illustrate the consequences of this choice with the example of Bloch wave $\mathrm{II}_{0.352,0}$. In the homogenous medium, this wave represents the electromagnetic plane wave with the wave vector $\mathbf{k}_{n^*,m^*}=(-0.648,0)$. Yet it is described by the wave vector $\mathbf{k}=(0.352,0)$ after the band folding. Consequently, the scalar product $\mathbf{k}\cdot\mathbf{v_g}$ is found to be negative, although this wave propagates in a usual homogenous medium. This contradiction results from the artificial band folding, which assigns an unjustified importance to the wave vector of the first BZ. The correct choice for $\mathbf{k}$ is $\mathbf{k}_{n^*,m^*}$ for which the scalar product $\mathbf{k}\cdot\mathbf{v_g}$ is naturally positive.

When the same approach is applied to PhCs, Bloch waves of the second band must be characterized by the wave vector $\mathbf{k}_{n^*,m^*}$ located in the second BZ. With this choice, the scalar product $\mathbf{k}_{n^*,m^*}\cdot\mathbf{v_g}$ is always positive. This result indicates that there is no fundamental difference between the physical properties of the first and second bands. In particular, the negative sign of the product $\mathbf{k}\cdot\mathbf{v_g}$ reported in previous papers is a consequence of the band folding and has limited physical meaning. Thus

PhCs cannot be considered LHMs at the energies corresponding to the second band. To generalize this result, the sign of $\mathbf{k}_{n^*,m^*}\cdot\mathbf{v_g}$ has been calculated for the first bands of many types of PhC and has never been found to be negative. In conclusion, PhCs do not generally satisfy the standard definition of LHMs.

4. REFRACTION PROPERTIES OF TWO-DIMENSIONAL PHOTONIC CRYSTALS

Although negative refraction has been experimentally observed in PhCs,[15,16] the Fourier analysis performed above clearly demonstrates that PhCs are not LHMs. In this section we illustrate our Fourier analysis with the example of light refraction at the interface between an homogenous medium and a 2D-PhC. In particular, we show that negative refraction effects observed in PhCs result from the specific nature of Bloch waves.

Let us consider first the well-known case of a plane wave launched from air into a dielectric material. The refraction is described by the Snell–Descartes law, $n_1\sin(\theta_1)=n_2\sin(\theta_2)$, where n_1,θ_1 and n_2,θ_2 are the refractive index and direction of the incident and refracted beams, respectively. A graphical solution to this problem can be provided by EFS analysis. In homogenous media the EFSs consist of circles whose radii are proportional to both the refractive index of the material and the wave frequency ($|\mathbf{k}|=n\omega/c$). The EFSs corresponding to the energy of the incident plane wave are represented for the air and the dielectric in Figs. 12(a) and 12(b), respectively. The wave vector $\mathbf{k_t}$ of the refracted plane wave is defined by the continuity of the tangential component of the incident wave vector $\mathbf{k_i}$ across the interface ($k_\parallel$ conservation) because of the translational invariance of the system. The group velocity $\mathbf{v_t}$ is then given by the gradient vector of the EFS. In this case the EFS is a circle, so the propagation direction is always parallel to the wave vector. Note that the $k_\parallel$-conservation line crosses the EFS at point B: This plane wave is not excited in the dielectric with this geometry as it is backward propagating with respect to the interface.

A convenient way to extend the EFS analysis to light refraction into PhCs is to consider which plane waves impinging on a PhC are able to excite a given Bloch wave. Let us consider, for example, the Bloch wave $\mathrm{II}_{-0.42,-0.24}$ propagating in the strongly modulated 2D-PhC discussed in Section 3. Its graphical representation is depicted in Fig. 13(b). To excite this Bloch wave, the incident beam must satisfy two conditions. First, its energy must be conserved, so the incident plane wave must belong to the corresponding EFS in the homogenous medium, i.e., the circle in Fig. 13(a). Second, the parallel component of the wave vector must be conserved along the interface (x axis). Projecting the wave vectors $\mathbf{k}_{n,m}$ of Bloch wave $\mathrm{II}_{-0.42,-0.24}$ on this axis, we obtain the following series of parallel components:

$$k_{\parallel n,m}=\mathbf{k}_{n,m}\cdot\mathbf{e_x}=\mathbf{k}\cdot\mathbf{e_x}+m2\pi/a. \tag{20}$$

To generalize the $k_\parallel$-conservation rule, all these parallel components must be conserved along the interface, and the $k_\parallel$-conservation line in Fig. 12 must be replaced by a $k_\parallel$-conservation comb in Fig. 13. In particular, the incident plane wave must have a wave vector whose projection corresponds to one of the $k_{\parallel n,m}$ components. The conservation of the other components is provided by the backward-diffracted waves. The components that cross the circle in Fig. 13(a) are conserved with reflected plane waves ($\mathbf{k_{r1}}$ and $\mathbf{k_{r2}}$), and the others are conserved with evanescent

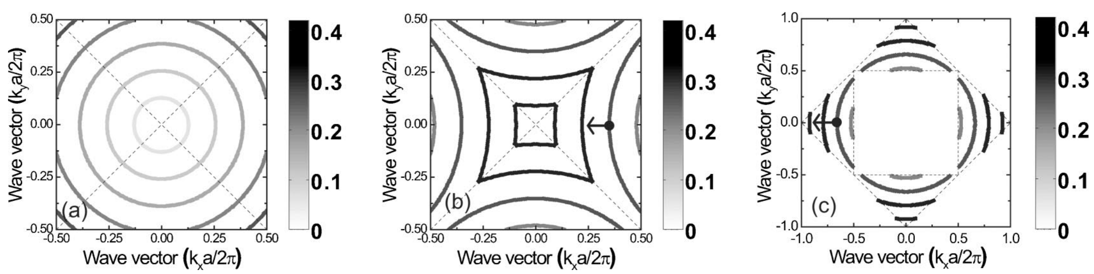

Fig. 10. EFS plots of a homogenous medium. (a) The EFS of the first band ($u\in[0,0.327]$) and (b) the standard representation of the EFS of the second band folded in the first BZ ($u\in[0.327,0.463]$). Bloch waves are characterized by the wave vector $\mathbf{k}=\mathbf{k}_{0,0}$, and the frequency increases outward (inward) in the first (second) band. Note that $\mathbf{v_g}$ and $\mathbf{k}$ point in opposite directions in case (b), thus erroneously suggesting left-handed material (LHM) behavior. (c) EFS of the second band in the second BZ. Here Bloch waves are characterized by the wave vector $\mathbf{k}_{n^*,m^*}$ of their dominant Fourier component (located in the second BZ). We see that the frequency increases outward and that $\mathbf{v_g}$ and $\mathbf{k}_{n^*,m^*}$ point in the same direction, thus indicating the expected right-handed behavior.

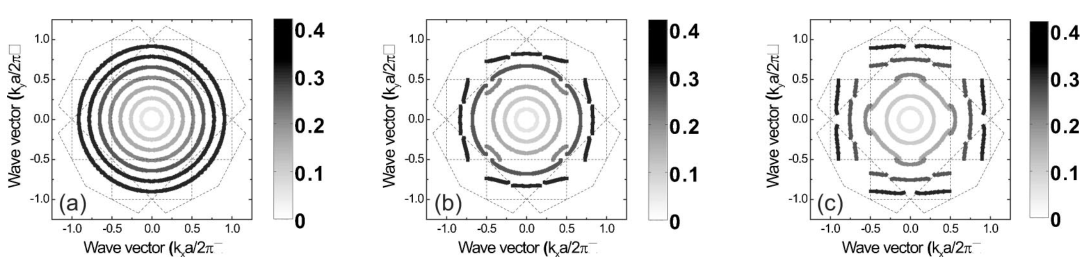

Fig. 11. Global EFS plots of the first four bands of (a) the homogenous medium, (b) the weakly modulated 2D-PhC, and (c) the strongly modulated 2D-PhC. Bloch waves are represented by the wave vector $\mathbf{k}_{n^*,m^*}$ of their dominant Fourier component. The continuous progression from a homogenous material to a strongly modulated material can be seen without any evidence of left-handed behavior.

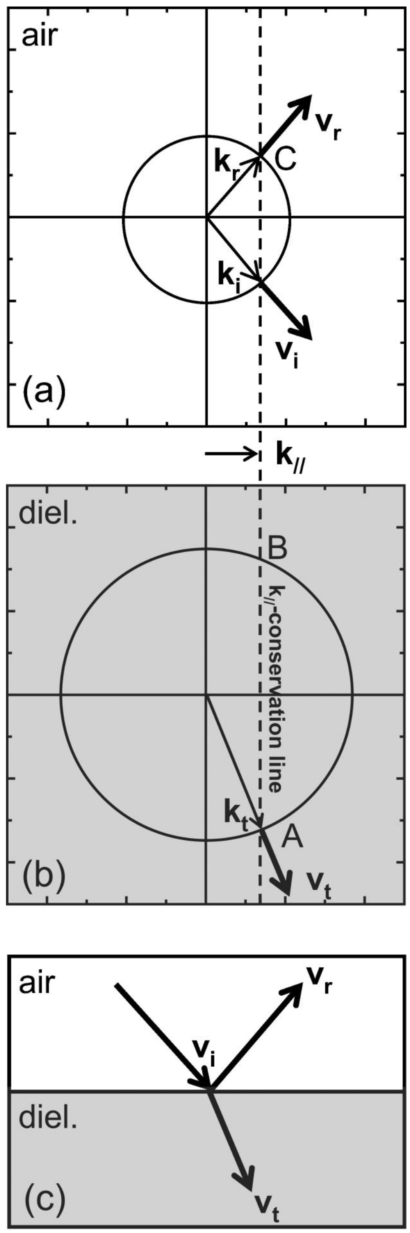

Fig. 12. Description of light refraction from air into a dielectric material by use of EFS analysis. (a) EFS in air. The wave vector $\mathbf{k_i}(\mathbf{k_r})$ and the group velocity $\mathbf{v_i}(\mathbf{v_r})$ of the incident (reflected) plane wave are indicated on the EFS by the thin and thick arrows, respectively. (b) EFS in the dielectric. The intersection of the $k_\parallel$-conservation line with the EFS (point A) gives the wave vector $\mathbf{k_t}$ of the transmitted plane wave. The other intersection (point B) corresponds to a backward-propagating wave that is not excited in this case. Point C gives the wave vector $\mathbf{k_r}$ of the reflected plane wave. (c) Summary of the propagation directions of the incident, transmitted, and reflected waves.

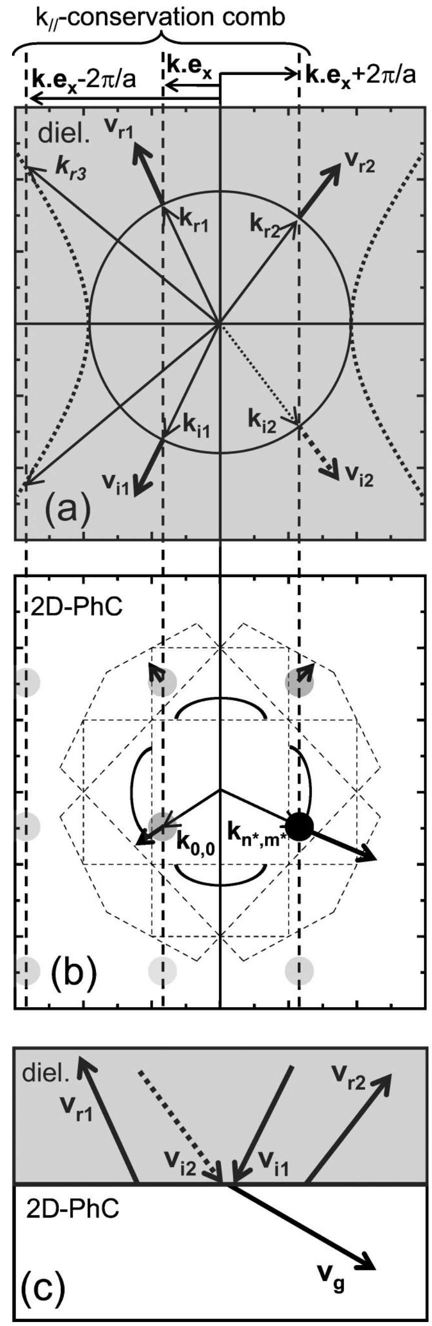

Fig. 13. Description of light refraction from a dielectric material into a 2D-PhC with EFS analysis. Here the $k_\parallel$-conservation line used in Fig. 12 must be replaced by a $k_\parallel$-conservation comb. We search for the incident plane waves that can excite a Bloch wave in the second band, e.g., $\mathrm{II}_{-0.42,-0.24}$ represented in (b). The standard solution is obtained by the conservation of the $k_\parallel$ component $\mathbf{k}\cdot\mathbf{e_x}$ and corresponds to the plane wave with the wave vector $\mathbf{k_{i1}}$ in (a). By use of the $k_\parallel$ component $\mathbf{k}\cdot\mathbf{e_x}+2\pi/a$, the incident plane wave with the wave vector $\mathbf{k_{i2}}$ can also excite the Bloch wave $\mathrm{II}_{0.3,-0.45}$. In both cases there are back-reflected plane waves characterized by the wave vectors $\mathbf{k_{r1}}$ and $\mathbf{k_{r2}}$. The other $k_\parallel$ components, e.g., $\mathbf{k}\cdot\mathbf{e_x}-2\pi/a$, are conserved by evanescent waves with imaginary $k_\perp$ components, e.g., $\mathbf{k_{r3}}$. The EFS for such waves are indicated in (a) by dashed curves for which the y axis has imaginary units. (c) A summary of the propagation directions of the incident, transmitted, and reflected waves. We observe that the incident plane wave $\mathbf{k_{i1}}$ is negatively refracted, unlike $\mathbf{k_{i2}}$.

waves having an imaginary $k_\perp$ component. According to diffraction theory, each incident plane wave whose wave vector's projection is equal to one of the $k_{\parallel n,m}$ is scattered by the periodic PhC structure into the Bloch wave $\mathrm{II}_{-0.42,-0.24}$. In this example, two possible incident plane waves fulfill this condition. The first corresponds to the plane wave with the wave vector $\mathbf{k_{i1}}$ and excites the Bloch wave through the parallel component $\mathbf{k}\cdot\mathbf{e_x}$; see Fig. 13(a). However, by use of the parallel component $\mathbf{k}\cdot\mathbf{e_x}+2\pi/a$, the plane wave with the wave vector $\mathbf{k_{i2}}$ can also be transmitted into the Bloch wave $\mathrm{II}_{-0.42,-0.24}$. Note that this second solution would be discarded with an EFS analysis restricted to the first BZ. In this case, only the conservation of the parallel component $\mathbf{k}\cdot\mathbf{e_x}$ is considered, and the ability to excite the Bloch wave through other parallel components is neglected. This result once again highlights the limits of an approach that focuses on the first BZ.

We can now qualitatively describe the refraction process at the interface between an homogenous medium and a PhC. When the incident plane wave impinges on the interface, the periodic lattice of holes acts as a diffraction grating, scattering the incident light forward (refraction) and backward (reflection). As shown by Foteinopoulou *et al.*,[14] after a transient time, the diffraction process reaches a steady state, which is the excited Bloch wave. Hence the Bloch wave is composed of the various waves resulting from the diffraction of the incident plane wave in the PhC, and therefore light refraction into PhCs should be considered a diffraction process.

Having established the physics of light transmission between an homogenous medium and a PhC, we can now consider the negative refraction effect observed in PhCs. In the example depicted in Fig. 13, the Bloch wave $\mathrm{II}_{-0.42,-0.24}$ can be excited independently by either plane wave $\mathbf{k_{i1}}$ or $\mathbf{k_{i2}}$. This Bloch wave lies in the second dispersion band, and its dominant wave vector $\mathbf{k}_{n^*,m^*}$ is located in the second BZ. The direction of its group velocity is dictated by the direction of $\mathbf{k}_{n^*,m^*}$ as shown in Section 3. When the solution $\mathbf{k_{i2}}$ is considered, the projections of $\mathbf{v_{i2}}$ and $\mathbf{v_g}$ point in the same direction, and positive (standard) refraction is obtained. Whereas the plane wave $\mathbf{k_{i1}}$ gives rise to the negative refraction because the projections on the interface of $\mathbf{v_{i1}}$ and $\mathbf{v_g}$ point is opposite directions. This demonstrates that whether positive or negative refraction occurs depends on the direction of the incident plane wave, and, equally, either can be observed for the same Bloch wave. It is important to note that an EFS analysis restricted to the first BZ would not point this out.

Finally, when one considers the solution $\mathbf{k_{i1}}$, the physical origin of the negative refraction can be considered. Once the Bloch wave $\mathrm{II}_{-0.42,-0.24}$ has been excited, its propagation direction is dictated by its dominant wave vector $\mathbf{k}_{n^*,m^*}$. Nevertheless, although the wave vectors $\mathbf{k}_{n,0}$ have negligible energetic contributions, they create the parallel component $\mathbf{k}\cdot\mathbf{e_x}$ used by $\mathbf{k_{i1}}$ to excite the Bloch wave. In conclusion, at the interface between a PhC and an homogenous material, a Bloch wave possess several $k_\parallel$ components that provide different excitation channels. Negative refraction occurs when the $k_\parallel$ component used for coupling and the $k_\parallel$ component of the dominant wave vector $\mathbf{k}_{n^*,m^*}$ are different and point in opposite directions. This situation can be compared with a blaze effect in a standard grating diffraction process.

5. CONCLUSION

We have shown that Fourier analysis of Bloch waves can provide a simple and intuitive method for understanding the propagative and refractive properties of light in PhCs. In previous studies the chosen wave-vector component to describe Bloch wave propagation has been taken from the first BZ. Although this is adequate for the first band, it can yield erroneous conclusions for higher-order bands. Unlike plane waves, Bloch wave propagation is not governed by a single wave vector because these waves possess multiple translational internal symmetries. A more appropriate choice is the wave vector of the plane wave that dominates the Fourier decomposition of the Bloch wave. Such a choice provides a common and consistent description of both the homogenous medium and the PhC. This approach always yields a positive sign for the scalar product $\mathbf{k}\cdot\mathbf{v_g}$ and points to the fact that PhCs are not intrinsically left handed. The negative refraction phenomenon observed in 2D-PhC originates from the specific properties of electromagnetic Bloch waves: The internal wave vector responsible for the propagation direction can differ from those responsible for the coupling with the incident plane wave. The excited Bloch wave results from the scattering of the incident radiation at the PhC interface, and therefore negative refraction must be understood as a diffraction phenomenon.

ACKNOWLEDGMENTS

The authors acknowledge P. S. J. Russell and C. M. Soukoulis for helpful discussions. This research was supported by the Swiss National Science Foundation in the framework of the research initiative National Centre for Competence in Research–Quantum Photonics and by the the Information Societies Technologies project "Photonic Crystal Integrated Circuits" (contract 1999-11239).

B. Lombardet, the corresponding author, may be reached by e-mail at benoit.lombardet@epfl.ch.

REFERENCES AND NOTES

1. J. Joannopoulos, R. Meade, and J. Winn, *Photonic Crystals: Molding the Flow of Light* (Princeton U. Press, Princeton, N.J., 1995).
2. E. Yablonovitch, T. J. Gmitter, and K. M. Leung, "Photonic band structure—the face-centered-cubic case employing nonspherical atoms," Phys. Rev. Lett. **67**, 2295–2298 (1991).
3. E. Yablonovitch, "Inhibited spontaneous emission in solid-state physics and electronics," Phys. Rev. Lett. **58**, 2059–2062 (1987).
4. M. Boroditsky, R. Vrijen, T. F. Krauss, R. Coccioli, R. Bhat, and E. Yablonovitch, "Spontaneous emission extraction and Purcell enhancement from thin-film 2-D photonic crystals," J. Lightwave Technol. **17**, 2096–2112 (1999).
5. C. Soukoulis, ed., *Photonic Crystals and Light Localization in the 21th Century* (Kluwer Academic, Dordrecht, The Netherlands, 2001).
6. J. G. Eden, ed., Special issue on photonic crystals, IEEE J. Quantum Electron. **38**, 724–963 (2002).
7. P. S. J. Russell, "Optics of Floquet–Bloch waves in dielectric gratings," Appl. Phys. B: Photophys. Laser Chem. **39**, 231–246 (1986).
8. P. S. J. Russell, "Bragg resonance of light in optical superlattices," Phys. Rev. Lett. **56**, 596–599 (1986).
9. R. Zengerle, "Light propagation in singly and doubly periodic planar wave-guides," J. Mod. Opt. **34**, 1589–1617 (1987).
10. P. S. J. Russell and T. Birks, "Bloch waves optics in photonic crystals: physics and applications," in *Photonic*

Band Gap Materials, C. M. Soukoulis, ed. (Kluwer Academic, Dordrecht, The Netherlands, 1996), pp. 71–91.
11. M. Notomi, "Theory of light propagation in strongly modulated photonic crystals: refractionlike behavior in the vicinity of the photonic band gap," Phys. Rev. B **62**, 10696–10705 (2000).
12. B. Gralak, S. Enoch, and G. Tayeb, "Anomalous refractive properties of photonic crystals," J. Opt. Soc. Am. A **17**, 1012–1020 (2000).
13. C. Luo, S. G. Johnson, J. D. Joannopoulos, and J. B. Pendry, "All-angle negative refraction without negative effective index," Phys. Rev. B **65**, 201104 (2002).
14. S. Foteinopoulou, E. N. Economou, and C. M. Soukoulis, "Refraction in media with a negative refractive index," Phys. Rev. Lett. **90**, 107402 (2003).
15. E. Cubukcu, K. Aydin, E. Ozbay, S. Foteinopolou, and C. M. Soukoulis, "Subwavelength resolution in a two-dimensional photonic-crystal-based superlens," Phys. Rev. Lett. **91**, 207401 (2003).
16. P. V. Parimi, W. T. T. Lu, P. Vodo, and S. Sridhar, "Photonic crystals—imaging by flat lens using negative refraction," Nature (London) **426**, 404 (2003).
17. A. Berrier, M. Mulot, M. Swillo, M. Qiu, L. Thylen, A. Talneau, and S. Anand, "Negative refraction at infrared wavelengths in a two-dimensional photonic crystal," Phys. Rev. Lett. **93**, 73902 (2004).
18. H. Kosaka, T. Kawashima, A. Tomita, M. Notomi, T. Tamamura, T. Sato, and S. Kawakami, "Superprism phenomena in photonic crystals," Phys. Rev. B **58**, 10096–10099 (1998).
19. T. Baba and M. Nakamura, "Photonic crystal light deflection devices using the superprism effect," IEEE J. Quantum Electron. **38**, 909–914 (2002).
20. L. J. Wu, M. Mazilu, T. Karle, and T. F. Krauss, "Superprism phenomena in planar photonic crystals," IEEE J. Quantum Electron. **38**, 915–918 (2002).
21. H. Kosaka, T. Kawashima, A. Tomita, M. Notomi, T. Tamamura, T. Sato, and S. Kawakami, "Self-collimating phenomena in photonic crystals," Appl. Phys. Lett. **74**, 1212–1214 (1999).
22. J. Witzens, M. Loncar, and A. Scherer, "Self-collimation in planar photonic crystals," IEEE J. Sel. Top. Quantum Electron. **8**, 1246–1257 (2002).
23. J. Witzens and A. Scherer, "Efficient excitation of self-collimated beams and single Bloch modes in planar photonic crystals," J. Opt. Soc. Am. A **20**, 935–940 (2003).
24. V. G. Veselago, "Electrodynamics of substances with simultaneously negative values of sigma and mu," Sov. Phys. Usp. **10**, 509–514 (1968).
25. K. Sakoda, *Optical Properties of Photonic Crystals* (Springer-Verlag, Berlin, 2001).
26. M. Plihal and A. A. Maradudin, "Photonic band-structure of 2-dimensional systems—the triangular lattice," Phys. Rev. B **44**, 8565–8571 (1991).
27. P. Yeh, "Electromagnetic propagation in birefringent layered media," J. Opt. Soc. Am. **69**, 742–756 (1979).
28. J. P. Dowling and C. M. Bowden, "Anomalous index of refraction in photonic bandgap materials," J. Mod. Opt. **41**, 345–351 (1994).
29. The computational implementation of this calculation requires a final scale transformation of the dimensionless vectors $\mathbf{e}_{n,m(\mathbf{k})}, \mathbf{d}_{n,m(\mathbf{k})}, \mathbf{h}_{n,m(\mathbf{k})}$ to normalize $\mathbf{h}_{n,m(\mathbf{k})}$. Indeed, when the software resolves the eigenvalues problem in Eq. (19), it generally normalizes the eigenvector $\mathbf{e}_{n,m(\mathbf{k})}/\mathbf{k}_{n,m}$.
30. B. Lombardet, L. A. Dunbar, R. Ferrini, and R. Houdré, "Bloch wave propagation in two-dimensional photonic crystals: influence of the polarization," special issue on optical waveguide theory and numerical modeling, Opt. Quantum Electron. (to be published).
31. M. Qiu, L. Thylen, M. Swillo, and B. Jaskorzynska, "Wave propagation through a photonic crystal in a negative phase refractive-index region," IEEE J. Sel. Top. Quantum Electron. **9**, 106–110 (2003).